

Enhancement and suppression of active particle movement due to membrane deformations

Adam Hitin Bialus¹, Bhargav Rallabandi²  and Naomi Oppenheimer^{1,3} 

¹School of Physics and Astronomy, Tel Aviv University, Tel Aviv 6997801, Israel

²Department of Mechanical Engineering, University of California, Riverside, CA 92521, USA

³Center for Physics and Chemistry of Living Systems, Tel Aviv University, Tel Aviv 6997801, Israel

Corresponding authors: Naomi Oppenheimer, naomiop@gmail.com; Adam Hitin Bialus, hitinbialus@mail.tau.ac.il

(Received 14 April 2025; revised 28 August 2025; accepted 5 October 2025)

Microswimmers and active colloids often move in confined systems, including those involving interfaces. Such interfaces, especially at the microscale, may deform in response to the stresses of the flow created by the active particle. We develop a theoretical framework to analyse the effect of a nearby membrane on the motion of an active particle whose flow fields are generated by force-free singularities. We demonstrate our results on a particle represented by a combination of a force dipole and a mass dipole, while the membrane resists deformation due to tension and bending rigidities. We find that the deformation either enhances or suppresses the motion of the active particle, depending on its orientation and the relative strengths between the fundamental singularities that describe its flow. Furthermore, the deformation can generate motion in new directions.

Key words: membranes, propulsion, swimming/flying

1. Introduction

Interactions between surfaces and viscous flows are abundant both in nature and in engineering (Molaei *et al.* 2014; Barbish *et al.* 2022). A scenario of particular interest occurs when the flow field is produced by an active microswimmer. The coupling between the flow of a microswimmer and fixed boundaries – either rigid walls or non-deforming fluid interfaces – has been extensively studied in past years (Lauga *et al.* 2006;

Bhargav Rallabandi and Naomi Oppenheimer jointly supervised this work.

Berke *et al.* 2008; Nasouri & Elfring 2016; Lushi, Kantsler & Goldstein 2017; Lauga 2020). In such cases, the interactions are limited by the time-reversal symmetry of the Stokes equations (Frymier *et al.* 1995; Berke *et al.* 2008; Molaei *et al.* 2014).

More recent work has studied interactions between suspended particles and deformable surfaces. The coupling between flow and deformation leads to nonlinear effects, breaking time-reversal symmetry and resulting in rich behaviour (Montecucco & Rappuoli 2001; Lee *et al.* 2008; Trouilloud *et al.* 2008; Dias & Powers 2013; Rallabandi *et al.* 2018). Exploration of hydroelastic interactions and motions resulting from them is vital to our understanding of a multitude of different biological and artificial processes, such as the shape of elastic filaments during sedimentation (Stone & Duprat 2015), the wake generated in elastic sheets (Ledesma-Alonso *et al.* 2016; Arutkin *et al.* 2017; Domino *et al.* 2018), the rheology of a suspension of red blood cells (Secomb *et al.* 1986; Pozrikidis 2005; McWhirter, Noguchi & Gompper 2009; Freund 2014; Secomb 2017; Guckenberger *et al.* 2018), the lubrication of joints in limbs (Walker *et al.* 1968; Dowson & Jin 1986; Jin & Dowson 2005), blood flow in capillaries (Dzwiniel, Boryczko & Yuen 2003) and the movement of artificial microswimmers with flexible tails (Dreyfus *et al.* 2005).

When passive particles move near deformable surfaces, fluid–elastic interactions generate additional particle motions, including a ‘lift’ of the particle away from the surface (Bureau *et al.* 2023; Rallabandi 2024). These effects have been demonstrated experimentally (Wang, Dhong & Frechette 2015; Saintyves *et al.* 2016; Rallabandi *et al.* 2018) and theoretically (Sekimoto & Leibler 1993; Skotheim & Mahadevan 2004; Skotheim & Mahadevan 2005; Moriarty *et al.* 2008; Daddi-Moussa-Ider *et al.* 2016, 2017; Kargar-Estahbanati & Rallabandi 2021) for various elastic and viscoelastic surface responses. Careful experimental measurements on passive particles have shown that these fluid–elastic interactions are important down to the nanoscale (Davies *et al.* 2018; Zhang *et al.* 2020; Fares *et al.* 2024). This suggests that similar interactions may be relevant for active motion of microswimmers and synthetic active matter at the microscale. Indeed, a hydroelastic lift was predicted for active swimmers (Trouilloud *et al.* 2008) near fluid interfaces, while recent work has analysed other aspects of active swimming near soft interfaces (Nambiar & Wettlaufer 2022; Jha, Amarouchene & Salez 2025; Garai *et al.* 2025).

In this work, we aim to understand how the presence of a nearby membrane changes the swimming behaviour of an active particle. Biological membranes are ubiquitous and their out-of-plane deformations are controlled by a bending rigidity and a membrane tension. The flow generated by a nearby microswimmer can, in principle, produce such deformations, which in turn affect the motion of the swimmer. For small membrane deformations, the problem can be mapped to that of a swimmer in the presence of a flat, rigid wall, with an induced slip velocity at the boundary. We exploit the Lorentz reciprocal theorem to find an analytical expression for the movement of a general class of active particles near deformable membranes. We then demonstrate our formalism for several models of active particles. We first consider self-propelled active particles and microorganisms. Then we consider active, but not self-propelled, particles (shakers) that can model active proteins near a membrane, such as actin and myosin. In particular, we focus on active particles described by a combination of a symmetric force dipole (a stresslet) of strength D and a mass dipole of strength q . We find that the membrane deformation can either be towards or away from the particle, depending on the orientation of the force and mass dipoles. This deformation can either enhance or suppress active motion along both x (parallel to the membrane) and z (perpendicular to the membrane), depending on the relative strength of the force and mass dipoles and their orientation. Moreover, the deformation can generate new movement both parallel and perpendicular to the membrane. We find that for a self-propelled particle, the interactions are inherently

long-ranged and depend on the gradient of the membrane's deformation, whereas for shakers, the interaction depends heavily on the deformation directly below the particle. For a self-propelled particle, these effects scale linearly with the dipole strength, while for shakers, the effect is quadratic in this strength. We study how these interactions vary with the membrane tension relative to its bending rigidity.

The rest of this paper is organised as follows. In § 2.1, we introduce the problem set-up and governing equations. In § 2.2, we derive a method of using the reciprocal theorem to extract the velocity correction for spherical active particles. Section 3.1 describes the active particle used for our numerical calculations and § 3.2 discusses how symmetries affect the results. Section 3.3 provides results for self-propelled particles and § 3.4 explores shakers in the different limits of the relative strength $q/|D|h$, h being the distance of the active particle from the membrane. Lastly, in § 4, we discuss the results, provide potential applications and suggest further research directions.

2. Background

2.1. Problem set-up

We consider a spherical active particle of radius a placed at $\mathbf{R} = \{0, 0, h\}$, where $h > 0$ is the height above an elastic membrane. In its equilibrium state, the membrane is planar and spans the xy plane. The particle translates with velocity \mathbf{V} in a viscous fluid of viscosity η . The particle's motion creates a flow that deforms the membrane. The deformation of the membrane then induces a secondary flow field, which in turn affects the motion of the particle. We are interested in solving for this effect under the condition of small membrane deformations.

In the limit of low Reynolds numbers ($a\rho|\mathbf{V}|/\eta \ll 1$, with ρ being the fluid density), the velocity field \mathbf{v} and stress field $\boldsymbol{\sigma}$ are governed by the Stokes equations (Leal 2007; Nambiar & Wettlaufer 2022),

$$\nabla \cdot \mathbf{v} = 0, \quad \nabla \cdot \boldsymbol{\sigma} = \mathbf{0}, \quad (2.1)$$

where $\boldsymbol{\sigma} = -\mathbf{I}p + \eta(\nabla\mathbf{v} + (\nabla\mathbf{v})^T)$ is the fluid stress tensor produced by the pressure field p and flow field \mathbf{v} (here, \mathbf{I} is the identity tensor in \mathbb{R}^3). The flow field due to the active particle will then create deformations in the membrane $\mathbf{u}(\mathbf{x}_W, \mathbf{R}, t)$, where \mathbf{x}_W represents a point in the plane of the undeformed membrane. We focus only on out-of-plane deformation, so $\mathbf{u} = \{0, 0, u_z\}$. The elastic, no-slip membrane has bending rigidity κ_B , surface tension T and is initially flat on the xy plane. The deformation satisfies the linearised Helfrich model (Helfrich 1973),

$$[\kappa_B \nabla_{||}^4 - \nabla_{||} \cdot (T \nabla_{||})]u_z = \sigma_{zz}, \quad (2.2)$$

with $\nabla_{||} = \{\partial_x, \partial_y, 0\}$ being the gradient operator in the plane of the undeformed membrane. No-slip conditions on the membrane–fluid interface are

$$\frac{d}{dt}(\mathbf{x}_W + \mathbf{u})|_{\mathbf{x}_W} = \mathbf{v}|_{\mathbf{x}_W + \mathbf{u}}, \quad (2.3)$$

where (d/dt) represents a material derivative.

2.2. General integral result

To find the induced velocity due to the membrane deformation, we invoke a perturbation solution for small membrane deformations and exploit the Lorentz reciprocal theorem. We introduce a dimensionless parameter Λ as the ratio of the characteristic deformation

amplitude to the distance of the swimmer from the membrane, i.e. $u_z = O(\Lambda h)$. We will later define Λ in terms of the details of the flow generated by the swimmer, which will generally be dominated by a force dipole. We then write the flow velocity as $\mathbf{v} = \mathbf{v}_0 + \mathbf{v}_1$, where \mathbf{v}_0 is the flow field of a particle near a flat, rigid, no-slip wall, and $|\mathbf{v}_1| \ll |\mathbf{v}_0|$ is the deformation-induced velocity which is a linear function of Λ . For the rest of the paper, the subscript 0 refers to quantities of an active particle near a flat, rigid, no-slip wall, whereas the subscript 1 refers to solutions linear in Λ . The reciprocal theorem relates the cross-dissipation of energy between two fields, the stress and velocity fields in the problem of interest, and those of a model flow field. It provides an integral equation that allows us to extract desired information on the problem at hand, such as force and particle velocity, from a model problem. The model problem we use is that of a Stokes flow produced by a rigid spherical particle of radius a moving with velocity $\hat{\mathbf{V}}$ due to an external force $\hat{\mathbf{F}}$ either parallel or perpendicular to a flat, no-slip rigid wall located at the xy plane. The induced velocity and stress fields of the model problem are denoted by $\hat{\mathbf{v}}$ and $\hat{\boldsymbol{\sigma}}$, respectively.

We expand out the particle swimming velocity \mathbf{V} , the fluid velocity \mathbf{v} and the stress $\boldsymbol{\sigma}$ as

$$(\mathbf{V}, \mathbf{v}, \boldsymbol{\sigma}) = (\mathbf{V}_0, \mathbf{v}_0, \boldsymbol{\sigma}_0) + (\mathbf{V}_1, \mathbf{v}_1, \boldsymbol{\sigma}_1) + \dots \quad (2.4)$$

We recall once again that quantities with subscript 1 are linear in the deformation parameter Λ . The swimming velocity near a rigid wall is \mathbf{V}_0 , which is modified by \mathbf{V}_1 due to the deformation. By linearity, the first-order fields satisfy the Stokes equations (2.1). Since we are interested in the deformation-related contribution to swimming, \mathbf{V}_1 , we apply the reciprocal theorem to relate the model flow to the first-order fields $\mathbf{v}_1, \boldsymbol{\sigma}_1$ (Lorentz 1896; Leal 2007; Kim & Karrila 2013),

$$\int_S \mathbf{n} \cdot \boldsymbol{\sigma}_1 \cdot \hat{\mathbf{v}} \, dS = \int_S \mathbf{n} \cdot \hat{\boldsymbol{\sigma}} \cdot \mathbf{v}_1 \, dS. \quad (2.5)$$

Here, the boundary S comprises three distinct parts: the boundary of the particle S_P , the boundary at the wall S_W and the boundary at infinity S_∞ . The integrals at infinity vanish due to the decay of the flow and stress fields away from the particle. On the left-hand side, the integral at the wall, S_W , vanishes due to the no-slip condition satisfied by the model flow. Due to the boundary condition on the particle satisfied by the model problem, the contribution of the integral on S_P , on the left-hand-side of (2.5), is $\hat{\mathbf{V}} \cdot \int_{S_P} \mathbf{n} \cdot \boldsymbol{\sigma}_1 \, dS$, which vanishes identically since the self-propelled particle is force-free.

We thus focus on the right-hand side of (2.5), which yields

$$-\mathbf{V}_1 \cdot \int_{S_P} \mathbf{n} \cdot \hat{\boldsymbol{\sigma}} \, dS = \mathbf{V}_1 \cdot \hat{\mathbf{F}} = \int_{S_W} \mathbf{n} \cdot \hat{\boldsymbol{\sigma}} \cdot \mathbf{v}_1 \, dS, \quad (2.6)$$

where $\mathbf{V}_1 = \mathbf{v}_1|_{S_P}$ is the first-order correction to the particle's velocity due to the membrane deformation. Also, $\hat{\mathbf{F}}$ is the force exerted by the particle in the model problem on the fluid; the change in sign in the last step stems from the orientation of \mathbf{n} into the fluid.

To finish the calculation, we evaluate the right-hand side of (2.6). To that end, we first establish the velocity correction \mathbf{v}_1 at the undeformed wall surface S_W to first order in Λ . The no-slip conditions on the membrane, (2.3), provide a link between the flow \mathbf{v} and the membrane deformation \mathbf{u} . We write out the material derivative on the left-hand side in terms of partial derivatives and expand the right-hand side in a Taylor expansion to obtain

$$\mathbf{v}_0(\mathbf{x}_W) + \frac{\partial}{\partial t} \mathbf{u} + \mathbf{V} \cdot \nabla_R \mathbf{u} = \mathbf{v}(\mathbf{x}_W) + \mathbf{u} \cdot \nabla \mathbf{v}(\mathbf{x}_W) + \dots, \quad (2.7)$$

where $(d\mathbf{x}_W/dt) = \mathbf{v}_0 = \mathbf{0}$ is the velocity at the plane in the undeformed configuration and $(\nabla_R \mathbf{u})_{ij} = \partial_{R_i} u_j$, \mathbf{R} being the position of the particle. We assume that the deformation is advected quasi-statically by the moving particle and that transient relaxation effects are fast. Invoking the expansion in (2.4) and retaining all terms up to a linear order in the deformation, we obtain the velocity at the wall as

$$\mathbf{v}_1|_{\mathbf{x}_W} = \mathbf{V}_0 \cdot \nabla_R \mathbf{u} - \mathbf{u} \cdot (\nabla \mathbf{v}_0)|_{\mathbf{x}_W}. \quad (2.8)$$

The ‘slip velocity’ in (2.8) stems from the deformation. That is, to first order in the deformation, the problem is identical to solving for the movement of the particle near a flat, rigid wall, with an effective slip velocity, given by (2.8), at the boundary.

The last step is then to solve for the deformation \mathbf{u} using (2.2), which to first order in Λ and assuming that tension is uniform is simply

$$(\kappa_B \nabla_{||}^4 - T \nabla_{||}^2) u_z = \sigma_{0,zz}. \quad (2.9)$$

Note that any non-homogeneity in T will arise purely due to the deformation. Thus, terms of the form $\nabla_{||} T$ will be of first order in Λ and will lead to a velocity correction of second order in Λ which can be neglected to first order. Finally, we arrive at the equation for the velocity correction,

$$\mathbf{V}_1 \cdot \hat{\mathbf{F}} = \int_{S_W} \mathbf{n} \cdot \hat{\boldsymbol{\sigma}} \cdot (\mathbf{V}_0 \cdot \nabla_R \mathbf{u} - \mathbf{u} \cdot \nabla \mathbf{v}_0) dS. \quad (2.10)$$

This equation provides a direct link between the particle’s velocity due to the deformation, \mathbf{V}_1 , and the other known quantities of the problem, namely \mathbf{V}_0 , \mathbf{v}_0 , \mathbf{u} and $\hat{\boldsymbol{\sigma}}$. The above-mentioned result is general to all force-free active particles, and is therefore applicable to a plethora of active particles and microswimmers, provided that the zeroth-order solution near a no-slip wall is known. Furthermore, due to the linearity of (2.2) and (2.1), given a swimmer model comprising a set of N singularities centred at \mathbf{R} , the solution to the velocity correction is readily given by

$$\mathbf{V}_1 \cdot \hat{\mathbf{F}} = \int_{S_W} \mathbf{n} \cdot \hat{\boldsymbol{\sigma}} \cdot \sum_{i=1}^N \sum_{j=1}^N \left(\mathbf{V}_0^i \cdot \nabla_R \mathbf{u}^j - \mathbf{u}^j \cdot \nabla \mathbf{v}_0^i \right) dS, \quad (2.11)$$

where we assume that each singularity translates with velocity \mathbf{V}_0^i , producing velocity and deformation fields \mathbf{v}_0^i and \mathbf{u}^i . Equation (2.11) forms the main result of this paper and gives a general expression for the velocity of an active force-free particle due to a nearby interfacial deformation.

3. Velocity induced by membrane deformation

In this section, we present the solutions to (2.11) for a variety of model particles. We will first consider an active particle that has a self-propulsion velocity and induces a flow by a force dipole and a mass dipole. As an example, we will take typical values measured for *E. coli* (Drescher *et al.* 2011). We will then consider a ‘shaker’ type of active particle (Marchetti *et al.* 2013), i.e. a particle that applies active stresses on its environment but is not self-propelled; examples can be active proteins such as myosin. For shakers, we will look at three cases: (a) a force and mass dipoles of equal strengths; (b) when the force dipole is dominant; and (c) when the mass dipole is dominant.

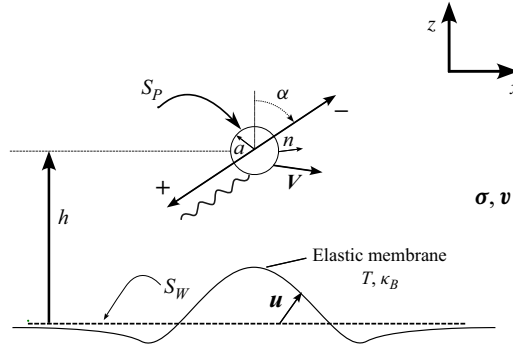


Figure 1. A schematic of the problem set-up of a microswimmer modelled as force and mass dipoles oriented at an angle α to an elastic membrane.

3.1. Active particle description

We first consider an active particle that self-propels with velocity $\mathbf{V}_{act} = V_{act}(\mathbf{e}_x \sin \alpha + \mathbf{e}_z \cos \alpha)$, which is realised in the absence of a membrane and is parallel to the direction of the force and mass dipoles. Near the membrane, the propulsion velocity becomes modified by interactions with the (rigid) wall, as well as corrections from the deformation. The wall does not deform due to \mathbf{V}_{act} itself, but by the flow that the particle creates. Since the particle is force-free, its far-away flow field decays as that of a force dipole (Drescher *et al.* 2011; Kurzthaler & Stone 2023). Furthermore, as the particle moves through the liquid, it displaces the fluid in front of it, ‘moving it’ to the back, resulting in a mass dipole-like behaviour (Witten & Diamant 2020; Kurzthaler & Stone 2023). Consequently, we represent the particle as a combination of mass and force dipoles (Trouilloud *et al.* 2008; Kurzthaler & Stone 2023). We solve (2.1) in the far-field limit, i.e. $h \gg a$. In free space, a force dipole generates flow and pressure fields of the form (Leal 2007; Kim & Karrila 2013)

$$v_i(\mathbf{r}) = \frac{D_{jk}}{8\pi\eta} \left(-\frac{r_i \delta_{jk}}{r^3} + 3\frac{r_i r_j r_k}{r^5} + \frac{r_k \delta_{ij} - r_j \delta_{ik}}{r^3} \right), \quad p(\mathbf{r}) = \frac{D_{jk}}{4\pi} \left(\frac{3r_j r_k}{r^5} - \frac{\delta_{jk}}{r^3} \right), \quad (3.1)$$

where $\mathbf{r} = \mathbf{x} - \mathbf{R}$ is the relative position vector of a field point \mathbf{x} and the particle’s position \mathbf{R} , and repeated indices are summed over. Here, \mathbf{D} is a tensor product of an orientation vector \mathbf{v}_{or} and a force unit vector \mathbf{v}_F . For a symmetric force dipole (stresslet), \mathbf{D} takes the general form $\mathbf{D} = D(\mathbf{v}_F \mathbf{v}_{or} + \mathbf{v}_{or} \mathbf{v}_F)$, where D is a dipole strength. We consider swimmers whose force and orientation vectors are the same, i.e. $\mathbf{v}_{or} = \mathbf{v}_F = \{\sin(\alpha), 0, \cos(\alpha)\}$, resulting in the dipole tensor

$$\mathbf{D} = D \begin{pmatrix} \sin^2(\alpha) & 0 & \sin(\alpha) \cos(\alpha) \\ 0 & 0 & 0 \\ \sin(\alpha) \cos(\alpha) & 0 & \cos^2(\alpha) \end{pmatrix}, \quad (3.2)$$

where we have chosen the dipole to lie in the xz plane without loss of generality. The angle α represents the orientation of the swimmer with respect to the z axis (figure 1). For the effect of the deformation on α , see Garai *et al.* (2025). We name the D_{11} (D_{33}) component of the tensor the parallel (perpendicular) term because for $\alpha = \pi/2$ ($\alpha = 0$), this is the only non-zero term. We call D_{13} and D_{31} the off-diagonal terms. Figure 2 shows

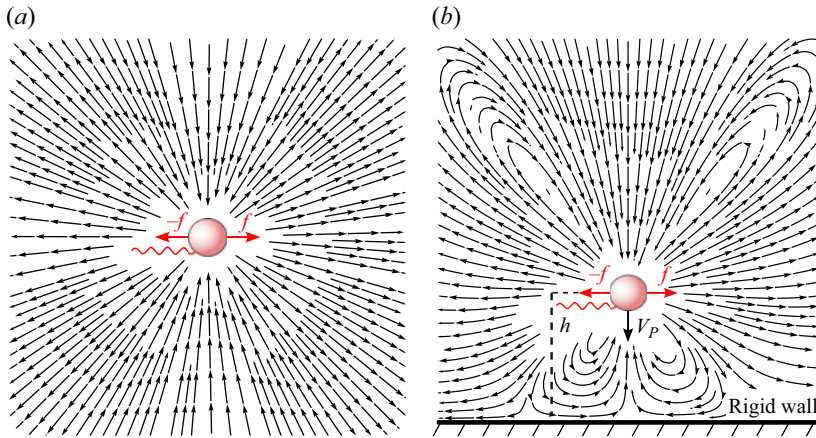


Figure 2. (a) Velocity field of a force dipole in free space. (b) Velocity field of a force dipole pointing parallel to a flat, rigid, no-slip boundary.

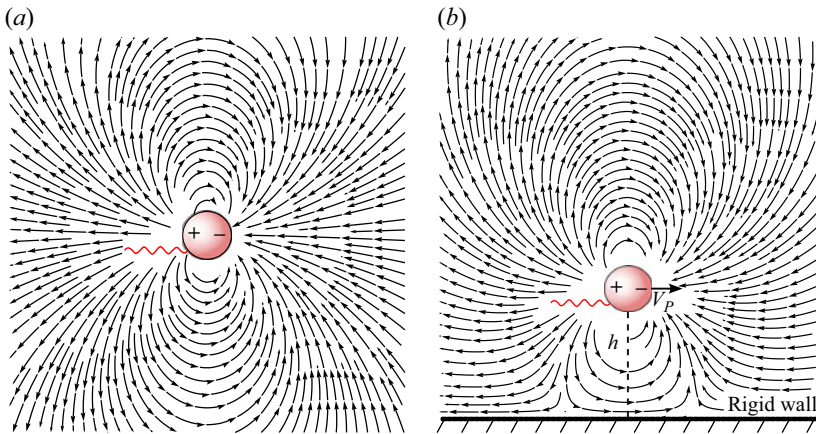


Figure 3. (a) Velocity field of a mass dipole in free space. (b) Velocity field of a mass dipole pointing parallel to a flat, rigid, no-slip boundary.

the flow fields generated by (a) a free stresslet and (b) a stresslet placed parallel to a no-slip wall. A mass dipole in free space generates a flow (Leal 2007; Kim & Karrila 2013),

$$v_i(\mathbf{r}) = \frac{q_j}{8\pi\eta} \left(\frac{\delta_{ij}}{r^3} - 3 \frac{r_i r_j}{r^5} \right), \quad p(\mathbf{r}) = 0, \quad (3.3)$$

with $\mathbf{q} = q \sin(\alpha)\mathbf{e}_x + q \cos(\alpha)\mathbf{e}_z$. We note that the active propulsion velocity generally includes contributions from higher-order singularities whose flow fields decay very fast away from the particle. In particular, for spherical particles, which we consider here, the active velocity is a quantity independent of both D and q .

Figure 3 shows the flow fields generated by (a) a free mass dipole and (b) a mass dipole placed parallel to a no-slip wall. A flat, rigid wall alters the flow due to no-slip on the surface of the wall. The flow field solution due to the presence of the flat wall is known for the stresslet and mass dipole, and the resultant velocity of the particle is then (Blake & Chwang 1974; Gimbutas, Greengard & Veerapaneni 2015)

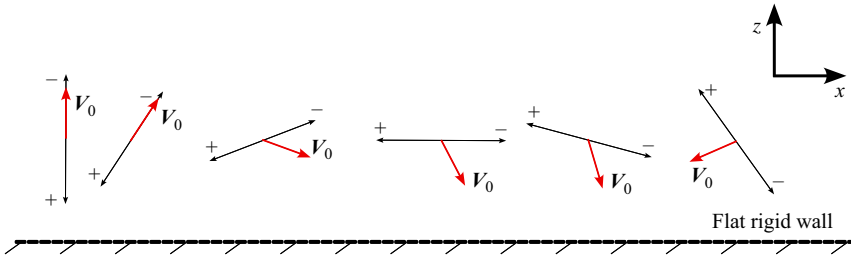


Figure 4. A schematic of the induced velocity due to a flat rigid wall V_0 as a function of the incident angle for a model particle.

$$\begin{aligned} V_0 &= V_{act} + \left(\frac{3D_{13}}{32\pi\eta h^2} + \frac{q_1}{32\pi\eta h^3} \right) \mathbf{e}_x + \left(\frac{3}{64\pi\eta h^2} [2D_{33} - D_{11}] + \frac{q_3}{8\pi\eta h^3} \right) \mathbf{e}_z \\ &= V_{act} + \frac{|D|}{8\pi\eta h^2} \left[\frac{\sin \alpha}{4} (3 \cos \alpha + Q) \mathbf{e}_x + \left(\frac{3}{8} [2 \cos^2 \alpha - \sin^2 \alpha] + Q \cos \alpha \right) \mathbf{e}_z \right], \end{aligned} \quad (3.4)$$

where we introduce the dimensionless relative strength of the dipoles $Q = q/|D|h$. Equation (3.4) describes the interaction of the different singularities with a flat, rigid wall. Notice that the motion near a flat wall is not trivial. Depending on the incident angle α , the particle can be attracted or repelled from the wall through hydrodynamic interactions. Similarly, it can move either along positive or negative x depending on the angle. For a more thorough discussion, see [Appendix A](#) and Kurzthaler & Stone (2023). Even for a pure stresslet or a pure mass dipole, the wall will induce motion. A schematic depiction of the velocity due to a flat wall V_0 with $V_{act} = \mathbf{0}$ is shown in [figure 4](#). Let us note that the correction to the velocity from the deformation is nonlinear in Q , and so it is not possible to simply superimpose separate results for the force-dipole and the mass dipole. As we will show, the combined flows produce a non-trivial correction.

We wish to understand the effect of the deformation on the particle motion, characterising both the enhancement or suppression of the motion, as well as the generation of motion in new directions. For motion in the xz plane and neglecting in-plane deformations, we evaluate gradients of velocity at the wall and insert them into (2.11) to find

$$V_1 \cdot \hat{\mathbf{F}} = \int_{S_w} \left\{ \hat{\sigma}_{zz} \left(V_{0,z} \frac{\partial u_z}{\partial h} - V_{0,x} \frac{\partial u_z}{\partial x} \right) - u_z \left(\hat{\sigma}_{zx} \frac{\partial v_{0,x}}{z} + \hat{\sigma}_{zy} \frac{\partial v_{0,y}}{\partial z} \right) \right\} dS. \quad (3.5)$$

We rescale all lengths by a characteristic height h_0 and define $d = h/h_0$ to be the dimensionless height. Furthermore, we rescale the velocity and stress fields by a characteristic velocity V_P ,

$$\mathbf{v} = V_P \mathbf{v}^* \quad \text{and} \quad \boldsymbol{\sigma} = \frac{V_P \eta}{h_0} \boldsymbol{\sigma}^*, \quad (3.6)$$

where $*$ indicates a dimensionless quantity. We then define the dimensionless parameter Λ , which controls the amplitude of the membrane's deformation, as

$$\Lambda = \frac{|D|}{\kappa_B} \quad (3.7)$$

and the dimensionless deformation as

$$u_z = \Lambda h_0 u_z^*, \quad (3.8)$$

with the assumption that $\Lambda \ll 1$. We note that when $\Lambda = 0$, the membrane is flat and we recover the case of a rigid flat wall. To evaluate the integral of (3.5) numerically, we need to know the stress field of the model problem $\hat{\sigma}$. At the wall, this model flow is dominated by that of a point force (Stokeslet) with $\hat{F} = 6\pi\eta a \hat{V}$. We thus scale the quantities in the model problem as

$$\hat{v} = \frac{a\hat{V}}{h_0} \hat{v}^* \quad \text{and} \quad \hat{\sigma} = \frac{a\hat{V}p_\eta}{h_0^2} \hat{\sigma}^*, \quad (3.9)$$

where $\hat{V} = |\hat{V}|$, and the solution for the above quantities is given by Blake (1971). Lastly, we rescale (3.5) to write

$$\mathbf{V}_1 \cdot \hat{\mathbf{V}} = \frac{DV_P}{6\pi\kappa_B} \int_{S_W} \hat{\sigma}_{zz}^* \left(V_{0,z}^* \frac{\partial u_z^*}{\partial d} - V_{0,x}^* \frac{\partial u_z^*}{\partial x^*} \right) - u_z^* \left(\hat{\sigma}_{zx}^* \frac{\partial v_{0,x}^*}{\partial z^*} + \hat{\sigma}_{zy}^* \frac{\partial v_{0,y}^*}{\partial z^*} \right) dS^*. \quad (3.10)$$

To find the deformation, we define the Fourier transform of a function $f(r, \phi)$ on the two-dimensional plane as

$$\mathcal{F}[f](k, \theta) = \tilde{f}(k, \theta) = \int_0^\infty \int_0^{2\pi} r f(r, \phi) e^{-irk \cos(\phi - \theta)} dr d\phi. \quad (3.11)$$

A Fourier transform of (2.9) leads to

$$\tilde{u}_z^* = \frac{V_P h_0^2 \eta}{|D|} \frac{\tilde{\sigma}_{0,zz}^*}{k^4 + \tau k^2}, \quad (3.12)$$

where we defined the dimensionless tension $\tau = Th^2/\kappa_B$. We evaluate (3.12) exactly and then perform a numerical inverse Fourier transform to find u_z^* . We then insert this result into (3.10) and evaluate the integral to obtain the component of \mathbf{V}_1 along a desired direction $\hat{\mathbf{V}}$; it is convenient to choose $\hat{\mathbf{V}} = \mathbf{e}_x$ or \mathbf{e}_z to obtain velocities along these directions. Finally, we set $d = 1$ without loss of generality (this merely picks the arbitrary length scale h_0).

3.2. Symmetries

The deformation due to the stresslet components is presented in figure 5. A detailed calculation in Appendix A shows that the deformation due to a mass dipole is identical to the deformation of the force dipole up to a factor of h . Symmetric deformations are produced by the parallel stresslet D_{11} , the perpendicular stresslet D_{33} and the perpendicular mass dipole q_3 . Conversely, both the off-diagonal terms, D_{13} and D_{31} , and the parallel mass dipole, q_1 , generate antisymmetric deformations. The velocity \mathbf{V}_1 is quadratic in the singularity strengths since it depends both on the stress and the deformation which, in turn, depends on the stress (cf. (3.10) and (3.12)). We separate these quadratic combinations into self-terms (a result of a single singularity) and cross-terms (interaction between singularities). To provide intuition for which terms contribute to the velocity, we inspect the terms of (3.10). The D_{11} , D_{33} and q_3 terms result in a symmetric deformation under $\phi \rightarrow -\phi$, while the deformation due to the D_{13} , D_{31} and q_1 terms is antisymmetric (table 1). If $\hat{\sigma}_{zz}$ is symmetric in ϕ , for a given singularity i , quadratic self-terms of the form $\hat{\sigma}_{zz} V_z^i \partial_h u_z^i$ always survive the integration. Similarly,

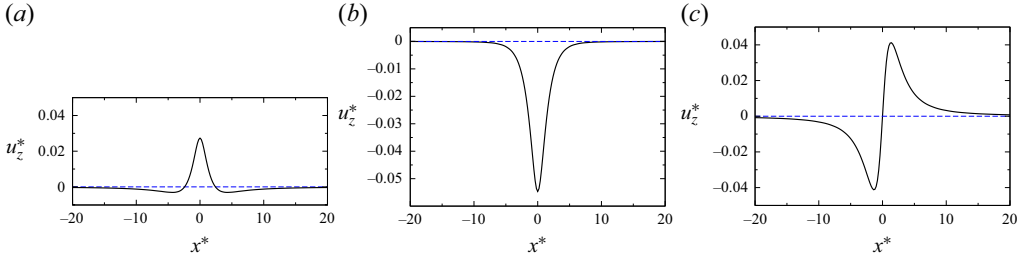


Figure 5. Dimensionless deformation of the membrane due to a stresslet located at $\{0, 0, 1\}$ with $\tau = 1$ as a function of dimensionless x^* . (a) A parallel stresslet. (b) A perpendicular stresslet. (c) Off-diagonal terms. The deformation due to a mass dipole is related by known factors to the deformation due to a stresslet (Appendix A).

cross-terms of the form $\hat{\sigma}_{zz} V_z^i \partial_h u_z^j$ survive the integration only if i, j represent either two symmetric singularities or two antisymmetric singularities. The same argument holds for terms of the form $u_z^i (\hat{\sigma}_{zx} \partial_z v_{0,x}^j + \hat{\sigma}_{zy} \partial_z v_{0,y}^j)$. If, however, $\hat{\sigma}_{zz}$ is antisymmetric, similar arguments show that only cross-terms between symmetric and antisymmetric singularities contribute.

3.3. Self-propelled particles

We first consider the correction to the velocity of a self-propelled particle ($V_{act} \neq 0$), which can model bacteria such as *E. coli*, chlamydomonas or other flagellated swimmers. We set the characteristic velocity $V_P = V_{act}$. Equation (3.10) suggests that the velocity correction scales as $V_1 \sim (V_{act} D / \kappa_B)$. Interestingly, this scale is independent of the distance h , suggesting long-range interactions. We will see later that the dependence on h is weak (logarithmic) when the tension is small. We rely on typical systems and set the ratios (Drescher *et al.* 2011)

$$\frac{D}{\eta a^2} \approx 25 |V_{act}| \quad \text{and} \quad \frac{h_0}{a} \approx 5. \quad (3.13)$$

We let $Q = 1$, so that the three terms contributing to the velocity of (3.4) are of comparable magnitudes. Notice that from (3.4), the particle's hydrodynamic interaction with a rigid flat wall already changes the particle's motion. Were the particle to move in free space, the change between swimming along positive or negative z would occur at $\alpha = 0.5\pi$. However, for the values specified previously, the particle moves away from the flat wall ($V_{0,z} > 0$) for $\alpha < 0.49\pi$ and towards it ($V_{0,z} < 0$) for $\alpha > 0.49\pi$ (more details are given in Appendix A.6).

3.3.1. Correction to the normal velocity

The deformation-induced velocity V_1 along the z direction (perpendicular to the membrane) as a function of dimensionless tension τ is presented in figure 6(a). Note that, as per (3.10), the correction is linear in $\Lambda = D / \kappa_B \ll 1$ and thus adds a small contribution to the total velocity $V = V_0 + V_1$. For small membrane tension, the correction scales as $V_1 \sim \log(\tau^{-1})$ (dashed line). Since $\tau = Th^2 / \kappa_B$, we have $V_1 \sim \log(\sqrt{\kappa_B / T} / h)$, where $\sqrt{\kappa_B / T}$ is a length scale set by a competition between bending and tension. Asymptotic expansions in this limit are tabulated in table 2 in the Appendix. For larger tensions, the velocity becomes smaller and scales by an additional power of h^{-2} . The normal velocity has a complicated dependence on the orientation angle α ; see figure 6(b). As discussed

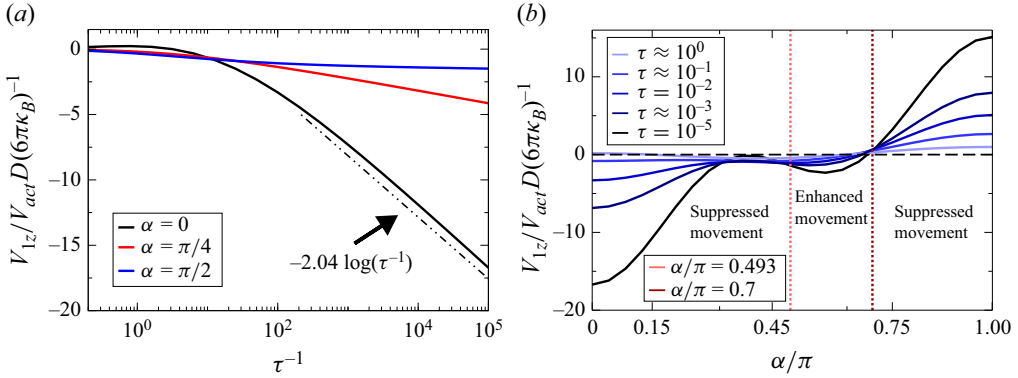


Figure 6. (a) Rescaled induced velocity along z of a self-propelled particle with force and mass dipole combination ($Q = 1$) as a function of dimensionless tension τ . Blue line is swimming parallel to the membrane, black line is perpendicular to membrane and red is swimming in $\alpha = \pi/4$. (b) Rescaled induced velocity along z of a self-propelled particle with force and mass dipole combination ($Q = 1$) as a function of orientation angle α . The terms enhancement and suppression are used to compare the velocity of the particle with the deformation, and the velocity near a flat, rigid, no-slip wall (see (3.4)).

previously, the particle moves away from the membrane ($V_{0,z} > 0$) for $\alpha < 0.49\pi$ and towards it ($V_{0,z} < 0$) for $\alpha > 0.49\pi$. This motion along z is suppressed by the deformation both for small angles ($\alpha < 0.49\pi$) and for large angles ($\alpha > 0.7\pi$). At intermediate angles ($0.49\pi < \alpha < 0.7\pi$), the deformation enhances the motion towards the membrane. Importantly, at the transition angle $\alpha = 0.49\pi$, $V_{0,z} = 0$, but the correction is not. That is, if the particle was placed next to a rigid flat wall at this angle, it would not move in the z direction, but a deformable membrane generates movement. The terms enhancement and suppression are used to compare the velocity of the particle with the deformation and the velocity near a flat, rigid, no-slip wall (3.4). In the previous example, suppressed motion along the positive z direction means that the particle is moving slower along positive z compared with the same particle placed near a flat, rigid wall.

3.3.2. Correction to the tangential velocity

The particle may either slow down or speed up along x due to the deformation, depending on α and τ (figure 7). As before, the correction scales as $\log \tau^{-1}$ for small tensions (see table 3 in the Appendix for more details). For $0 < \alpha < \pi$, the particle moves along $+x$ ($V_{0,x} > 0$) in the absence of deformation. For small membrane tensions, the deformation retards the self-propulsion along x for all orientations α . Conversely, for large tensions ($\tau \gtrsim 10^{-1}$), the deformation enhances motion when $0 < \alpha < 0.42\pi$, while it suppresses motion along x for larger orientation angles $0.42\pi < \alpha < \pi$.

3.4. Shakers

A shaker is an active particle that may drive flow but does not self-propel. Examples include active proteins near membranes. However, the flows that such particles create can interact hydrodynamically with nearby boundaries – including deformable ones – leading to ‘induced’ motion of a shaker (Mikhailov & Kapral 2015). Here, we demonstrate the effects of the membrane on an active, but not self-propelled particle ($V_{act} = \mathbf{0}$). We find that when the active velocity is negligible, the dominant contribution to the correction comes from the deformation directly below the particle. If the membrane is deformed towards the particle, its velocity will be enhanced, while if the deformation is away from the particle, it will be suppressed. In addition to the orientation angle and the dimensionless tension,

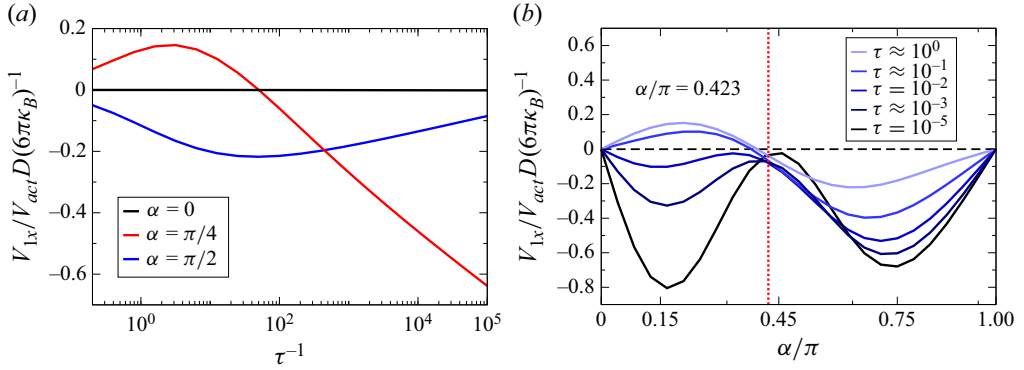


Figure 7. (a) Rescaled induced velocity along x of a self-propelled particle with force and mass dipole combination ($Q = 1$) as a function of dimensionless tension τ . Blue line is swimming parallel to the membrane, black line is perpendicular to membrane and red is swimming in $\alpha = \pi/4$. (b) Rescaled induced velocity along x of a self-propelled particle with force and mass dipole combination ($Q = 1$) as a function of orientation angle α .

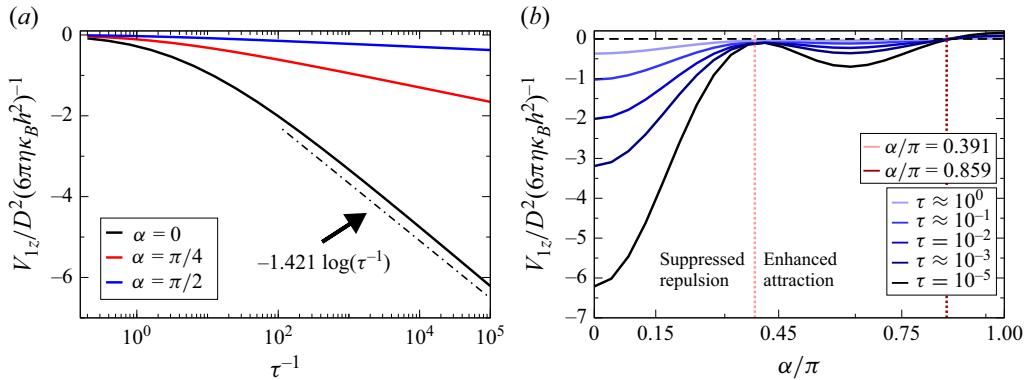


Figure 8. (a) Rescaled induced velocity along z of a force and mass dipole combination ($Q = 1$) as a function of dimensionless tension τ . Blue line is swimming parallel to the membrane, black line is perpendicular to membrane and red is swimming in $\alpha = \pi/4$. (b) Rescaled induced velocity along z of a force and mass dipole combination ($Q = 1$) as a function of orientation angle α .

the motion is controlled by the ratio of the mass and force dipole strengths, Q . We discuss these effects later, focusing on $Q = 1$ with further analysis provided in [Appendix A](#).

The natural velocity scale, which we also choose to be the characteristic velocity for non-dimensionalisation, is set by the dipole strength as $V_P = |D|/\eta h_0^2$. From (3.10), the velocity due to the deformation scales as $V_1 \sim (D^2/\eta\kappa_B h_0^2)$, up to a dimensionless function of τ .

3.4.1. Correction to the normal velocity

The induced velocity V_1 along the z direction as a function of dimensionless tension τ is presented in [figure 8\(a\)](#). For small surface tension, the velocity scales as $V_1 \sim \log \tau / h^2$ (see [table 2](#) in the Appendix for details). For most angles and tensions, the membrane deformation leads to a velocity correction towards the membrane. The exception occurs at α close to π , where the induced velocity is away from the membrane. We understand these behaviours by analysing some limiting cases. For small angles ($\alpha \approx 0$), the particle

is repelled from a rigid wall due to hydrodynamic interactions, according to (3.4). Meanwhile, the flow due to the particle is directed away from the particle towards the membrane (it is roughly that of a perpendicular stresslet), causing the membrane to deform away from the particle (similar to the situation depicted in figure 5b). We can therefore think of the situation with a deformable membrane as ‘moving the flat wall further away’, which from (3.4) suggests a suppressed repulsion for small α (see figure 8b). The reverse occurs when $\alpha = \pi/2$. The particle is attracted to a rigid wall according to (3.4). Furthermore, the flow is dominated by a parallel stresslet and so the membrane deformation is towards the particle, as indicated in figure 5(a). Thus, we can think of the wall as ‘moving closer’ to the particle as a consequence of deformation, strengthening the interaction and enhancing the attraction towards the membrane.

With these observations, we expect that the cross-over between enhancement and suppression occurs when the membrane deformation right below the particle, i.e. at the origin, vanishes. We denote the deformation due to the perpendicular stresslet and mass dipole by (u_z^\perp) , and the deformation due to the parallel stresslet as (u_z^\parallel) ; the parallel mass dipole does not deform the membrane at the origin. Thus, the deformation at the origin is

$$u_z|_{x=y=0} = ([\cos^2(\alpha) + Q \cos(\alpha)]u_z^\perp + \sin^2(\alpha)u_z^\parallel)|_{x=y=0}. \quad (3.14)$$

From (A5), (A6) and (A10), we find that $u_z^\perp = -2u_z^\parallel$ at the origin. Setting the deformation to zero at the origin provides us with an approximation for the cross-over orientation angle α_{cross} ,

$$\cos(\alpha_{cross}) = \frac{-Q + \sqrt{Q^2 + 3}}{3}. \quad (3.15)$$

For $Q = 1$, we obtain a prediction $\alpha_{cross} = 1.23 \approx 0.4\pi$ from (3.15). This is consistent with the detailed calculation in figure 8(b), which shows the velocity correction along z as a function of the incident angle α ; the predicted α_{cross} is indicated by the leftmost vertical red line. Indeed, at α_{cross} , the correction is small and it stems from the antisymmetric part of the deformation alone, which is zero at the origin, suggesting that the deformation at the origin is the most significant contributor to the velocity correction. Figure 9 shows α_{cross} as a function of the ratio Q . The cross-over angle is relatively insensitive to the tension τ , which is consistent with the prediction of (3.15), which depends only on the ratio $Q = q/|D|h$.

Lastly, for $\alpha/\pi \approx 0.86$ (rightmost vertical line in figure 8b), the deformation-induced velocity changes sign and becomes positive. We attribute this behaviour to a competition between the perpendicular terms of the stresslet and mass dipole, which either ‘push’ or ‘pull’ the particle away from or towards the membrane, but scale differently with h .

3.4.2. Correction to the tangential velocity

The tangential velocity due to the deformation can be either positive or negative depending on the angle (figure 10). As before, we understand the results from the symmetries of the different terms and from the shape of the deformation. For moderate α , it follows a similar pattern of suppressed or enhanced movement as the normal velocity, with a transition occurring for $\alpha/\pi \approx 0.39$. Interestingly, at $\alpha/\pi \approx 0.61$, the deformation induces particle motion, even though the particle does not move along x at this angle in the rigid case.

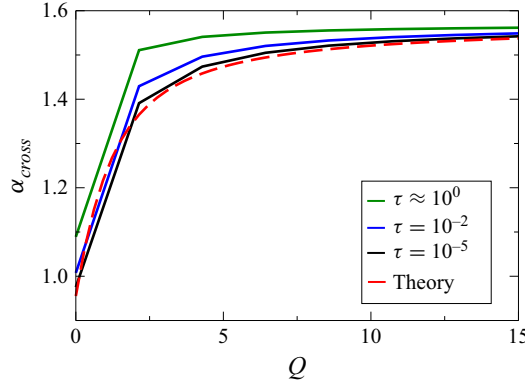


Figure 9. A plot of the crossing angle α_{cross} for a force and mass dipole combination as a function the relative strength Q .

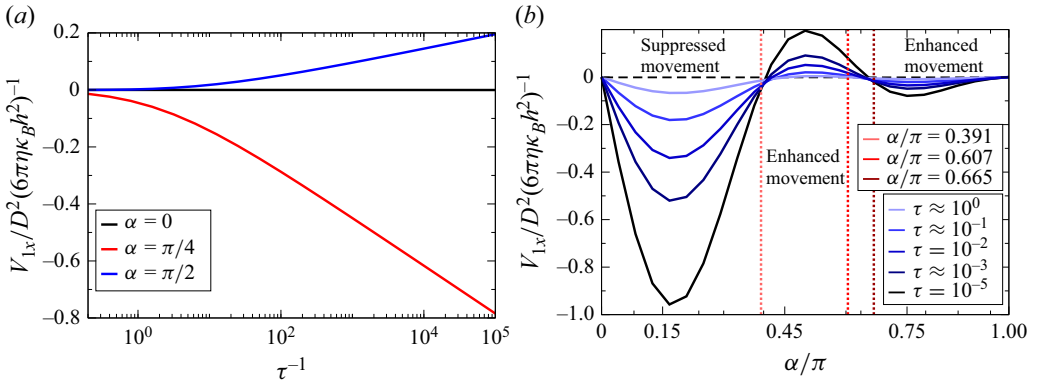


Figure 10. (a) Rescaled induced velocity along x of a force and mass dipole combination ($Q = 1$) as a function of dimensionless tension τ . Blue line is swimming parallel to the membrane, black line is perpendicular to membrane and red is swimming in $\alpha = \pi/4$. (b) Rescaled induced velocity along x of a force and mass dipole combination ($Q = 1$) as a function of orientation angle α .

3.4.3. Other limits of dipole and mass strengths

The regions of enhanced and suppressed motion depend on the dipole strength ratio Q . For small Q , the force dipole is dominant and the cross-over angle becomes approximately 0.3π (cf. figure 9 with $Q = 0$). The deformation induces a correction towards the surface for all α . When $\alpha < \alpha_{cross}$, the deformation suppresses the interaction relative to the undeformed case (repulsion), while for $\alpha > \alpha_{cross}$, it enhances the interaction (attraction). Motion along x mirrors the same pattern of enhancement and suppression, with a positive V_{1x} for $\alpha < \alpha_{cross}$ and negative V_{1x} for $\alpha > \alpha_{cross}$. When $Q \rightarrow \infty$, the force dipole is negligible and the mass dipole dominates. It is now necessary to choose the characteristic velocity as $V_P = q(\eta h_0^3)^{-1}$ leading to $\Lambda = q(h_0 \kappa_B)^{-1}$. Therefore, the correction velocity due to the deformation now scales as $V_1 \sim (q^2 / \eta \kappa_B h^4)$. In this case, the cross-over angle according to (3.15) is $\alpha_{cross} = \pi/2$ (cf. figure 9 with $Q = 15$). Along both normal and tangential directions, the effect of deformation from the mass dipole mirrors that of the stresslet, but with the modified cross-over angle. For a more detailed analysis of the effect of Q on the correction, see Appendices A.4 and A.5.

4. Discussion

In this work, we used the reciprocal theorem to derive an analytical expression for the first-order correction to the velocity of an active particle in the presence of an infinite elastic membrane with bending rigidity and surface tension. Our approach relies on far-field effects and small membrane deformation while allowing for arbitrary orientation with respect to the membrane, as long as no net forces act on the particle. We first present a particle modelled as a force and mass dipole combination with relative strength $Q = 1$ and active velocity V_{act} . We show the deformation can either enhance or suppress the motion of the particle associated with interactions with a rigid wall, depending on the incident angle α . When V_{act} is negligible, we develop an analytic expression to predict the value where the effect changes from suppression to enhancement and show that it agrees well with the detailed calculation. Furthermore, we find that deformation can generate movement along both z and x directions for certain incident angles. The calculations rely on small deformations such that $\Lambda \ll 1$. Indeed, many biological systems obey this constraint. For example, in the interaction between *E. coli* and white blood cells, where $\kappa_B \approx 500k_B T$ for white blood cells and $D \approx 250k_B T$ for *E. coli* resulting in $\Lambda = 0.5$ (Drescher *et al.* 2011; Fedosov, Fornleitner & Gompper 2012). Similarly, the dipole strength of myosin can be approximated to be of the order of a few $k_B T$ and the bending rigidity of a red blood cell $\kappa_B \approx 50k_B T$ giving $\Lambda \sim 0.1$ (Lampinen & Noponen 2005; Fedosov *et al.* 2012). If we take the tension rigidity T of a red blood cell to be roughly 10^{-6} N m^{-1} and the distance of myosin to the membrane $h \approx 10^{-9} \text{ m}$, we get $\tau = 10^{-3}$ and $V_{1,z} = 0.05V_{act}$ (Omori *et al.* 2012). Furthermore, myosin II proteins form filaments of ~ 30 particles near the membrane; therefore, the total interaction will be more appreciable, leading to an order of magnitude larger correction (Grewe & Schwarz 2020). The average correction as a function of the angle α can be calculated as $\langle V_{1,z} \rangle_\alpha = 1/2 \int_0^\pi V_{1,z}(\alpha) \sin \alpha d\alpha$. In other words, given a sparse swarm of active particles near an elastic membrane, we can find the average correction along z of the centre of mass. For a self-propelled swarm with $\tau = 10^{-5}$, the correction will be attractive and given by $-0.9V_{act}D/\kappa_B$. Similarly, for a sparse swarm of shakers, we find an average attraction of $-0.9D^2/\eta\kappa_B h_0^2$. Lastly, for pure force dipoles, we find $-0.3D^2/\eta\kappa_B h_0^2$. Surprisingly, for the particle models explored here, the correction along z is always attractive on average. Along the x direction for self-propelled particles with $\tau = 10^{-5}$, the average correction is $-0.4V_{act}D/\kappa_B$ and suppresses the existing motion.

The approach developed here can be used on a plethora of model swimmers, provided no net force is applied and the solution near a rigid no-slip wall is known. These calculations can be useful to better understand the behaviour of a variety of biological microswimmers, such as *E. coli*, or even robotic swimmers. The results here might be particularly important for synthetic biology, where one can fine-tune the bending and tension of the membrane (Tang *et al.* 2021). The effects of non-uniform bending rigidity of the membrane, e.g. due to the accumulation of cholesterol in the veins, can also be considered (Chakraborty *et al.* 2020). The complex motion of several particles near an elastic boundary can also be explored by extending formalisms similar to those developed here (Elfving & Lauga 2014).

Funding. This work was supported by NSF-BSF Grant No. 2023624 and NSF Grant No. 2328628.

Declaration of interests. The authors report no conflict of interest.

Appendix A. Calculation of velocity components and deformations

A.1. Force dipole

We wish to numerically solve the integral in (3.10). We first consider a pure force dipole. The rescaled velocity derivatives are (Gimbutas *et al.* 2015)

$$\partial_{z^*} v_{0,x}^*|_{s_w} = \begin{cases} -\frac{3r \cos(\phi)}{2\pi} \left(\frac{2}{(r^2+1)^{5/2}} - \frac{5r^2 \cos^2(\phi)}{(r^2+1)^{7/2}} \right) \sin^2(\alpha), & \text{parallel swimming} \\ -\frac{3r \cos(\phi)}{2\pi} \left(\frac{2}{(r^2+1)^{5/2}} - \frac{5}{(r^2+1)^{7/2}} \right) \cos^2(\alpha), & \text{perpendicular swimming} \\ \frac{3}{2\pi} \left(\frac{r^2 \cos^2(\phi)+1}{(r^2+1)^{5/2}} - \frac{10r^2 \cos^2(\phi)}{(r^2+1)^{7/2}} \right) \cos(\alpha) \sin(\alpha), & \text{off-diagonal terms} \end{cases}$$

$$\partial_{z^*} v_{0,y}^*|_{s_w} = \begin{cases} -\frac{3r \sin(\phi)}{2\pi} \left(\frac{2}{(r^2+1)^{5/2}} - \frac{5r^2 \cos^2(\phi)}{(r^2+1)^{7/2}} \right) \sin^2(\alpha), & \text{parallel swimming} \\ -\frac{3r \sin(\phi)}{2\pi} \left(\frac{2}{(r^2+1)^{5/2}} - \frac{5}{(r^2+1)^{7/2}} \right) \cos^2(\alpha), & \text{perpendicular swimming} \\ \frac{3 \cos(\phi) \sin(\phi) r^2}{2\pi} \left(\frac{1}{(r^2+1)^{5/2}} - \frac{10}{(r^2+1)^{7/2}} \right) \cos(\alpha) \sin(\alpha), & \text{off-diagonal terms,} \end{cases} \quad (\text{A1})$$

where we defined $x = r \cos(\phi)$, $y = r \sin(\phi)$ as the coordinates on the flat wall and we took $d = 1$. Next, to calculate the correction along z , the model problem is a Stokeslet pointing along z where the stress field $\hat{\sigma}^*$ is (Blake 1971; Blake & Chwang 1974)

$$\hat{\sigma}_{zz}^* = \frac{9}{(r^2+1)^{5/2}}. \quad (\text{A2})$$

Due to the symmetry of the model problem, we can write $\hat{\sigma}_{zx}^* = \hat{\sigma}_{zr}^* \cos(\phi)$ and $\hat{\sigma}_{zy}^* = \hat{\sigma}_{zr}^* \sin(\phi)$. Moreover, since $w_r = w_x \cos(\phi) + w_y \sin(\phi)$ for any vector \mathbf{w} , the second terms in (3.10) can be written as

$$u_z^* \hat{\sigma}_{zr}^* \partial_{z^*} v_{0,r}^*, \quad (\text{A3})$$

with

$$\hat{\sigma}_{zr}^* = -\frac{9r}{(r^2+1)^{5/2}}. \quad (\text{A4})$$

Lastly, we write the deformation in Fourier space

$$\tilde{u}_z^*(k, \theta) = \frac{dk^2 e^{-dk} \cos^2(\theta)}{k^4 + \tau k^2} \sin^2(\alpha) \quad \text{parallel swimming,} \quad (\text{A5})$$

$$\tilde{u}_z^*(k, \theta) = -\frac{dk^2 e^{-dk}}{k^4 + k^2 \tau} \cos^2(\alpha) \quad \text{perpendicular swimming} \quad (\text{A6})$$

and

$$\tilde{u}_z^*(k, \theta) = -\frac{2i dk^2 e^{-dk} \cos(\theta)}{k^4 + k^2 \tau} \cos(\alpha) \sin(\alpha) \quad \text{Off-diagonal terms,} \quad (\text{A7})$$


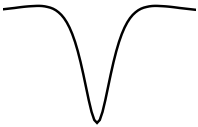


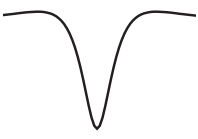
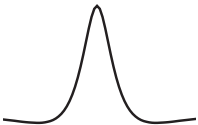
Singularity	Deformation scheme	Correction type
Parallel force dipole (D_{11})		Enhanced attraction
Perpendicular force dipole (D_{33})		Reduced repulsion
Off-diagonal terms (D_{13}, D_{31})		Generating attraction
Parallel mass dipole (q_1)		Generating attraction
Perpendicular mass dipole (q_3)($\alpha < \pi/2$)		Reduced repulsion
Perpendicular mass dipole (q_3)($\alpha > \pi/2$)		Enhanced attraction

Table 1. Result schemes by singularity.

and use Mathematica to numerically perform the inverse transform. Notice that at $r = 0$, the inverse Fourier transforms of (A5) and (A6) are identical up to a factor of -2 , which stems from the negative sign and the integration over $\cos^2(\theta)$. This implies that at the origin, the amplitude of the deformation due to the perpendicular term will be twice that of the parallel term.

We can understand which terms will survive the integration by a closer inspection of (3.10). We separate the interaction into quadratic terms (a result of a single singularity) and cross-terms (interaction between singularities). Notice that the parallel and perpendicular terms result in a symmetric deformation under $\phi \rightarrow -\phi$, while the deformation due to the off-diagonal terms is antisymmetric (cf. table 1). Moreover, $\partial_h u_z$ never breaks this symmetry while $\partial_x u_z$ reverses it. Now, since $\hat{\sigma}_{zz}$ is symmetric in ϕ , for a given singularity i , quadratic terms of the form $\hat{\sigma}_{zz} V_z^i \partial_h u_z^i$ always survive the integration. Similarly, cross-terms of the form $\hat{\sigma}_{zz} V_z^i \partial_h u_z^j$ only survive the integration if i, j represent either two symmetric singularities or two antisymmetric singularities. The same argument holds for terms of the form $u_z^i (\hat{\sigma}_{zx} \partial_z v_{0,x}^j + \hat{\sigma}_{zy} \partial_z v_{0,y}^j)$.

The calculation of velocity along the x direction is similar. Here, we choose the model problem to be a Stokeslet pointing along positive x . Now, the stress tensor $\hat{\sigma}^*$ is (Blake 1971; Blake & Chwang 1974)

$$\hat{\sigma}_{zz}^* = -\frac{9r \cos(\phi)}{(r^2 + 1)^{5/2}}, \quad \hat{\sigma}_{zx}^* = \frac{9r^2 \cos^2(\phi)}{(r^2 + 1)^{5/2}} \quad \text{and} \quad \hat{\sigma}_{zy}^* = \frac{9r^2 \cos(\phi) \sin(\phi)}{(r^2 + 1)^{5/2}}, \quad (\text{A8})$$

where now, we no longer have symmetry under $\phi \rightarrow \phi + \pi$ and we need both $\hat{\sigma}_{zx}^*$ and $\hat{\sigma}_{zy}^*$. Notice that the model problem is antisymmetric under $\phi \rightarrow -\phi$. A symmetry argument now shows that all quadratic terms will cancel and only cross-terms between symmetric and antisymmetric singularities will survive the integration of (3.10).

A.2. Mass dipole

For a mass dipole, the rescaled velocity derivatives are (Blake & Chwang 1974)

$$\partial_{z^*} v_{0,x}^*|_{s_w} = \begin{cases} -\frac{3}{2\pi} \left(\frac{5r^2 \cos^2(\phi)}{(r^2+1)^{7/2}} - \frac{1}{(r^2+1)^{5/2}} \right) & \text{parallel swimming,} \\ \frac{3r \cos(\phi)}{2\pi} \left(\frac{5}{(r^2+1)^{7/2}} - \frac{1}{(r^2+1)^{5/2}} \right) & \text{perpendicular swimming,} \end{cases} \quad (\text{A9})$$

$$\partial_{z^*} v_{0,y}^*|_{s_w} = \begin{cases} -\frac{15r^2 \sin(\phi) \cos(\phi)}{2\pi (r^2+1)^{7/2}} & \text{parallel swimming,} \\ = \frac{3r \sin(\phi)}{2\pi} \left(\frac{5}{(r^2+1)^{7/2}} - \frac{1}{(r^2+1)^{5/2}} \right) & \text{perpendicular swimming.} \end{cases}$$

The deformation terms are

$$\tilde{u}_z^*(k, \theta) = -\frac{k^2 e^{-dk}}{k^4 + k^2 \tau} \cos(\alpha) \quad \text{perpendicular swimming.} \quad (\text{A10})$$

Note that this is similar to the perpendicular terms of the force dipole, but with one less factor of d , and

$$\tilde{u}_z^*(k, \theta) = -\frac{ik^2 e^{-dk} \cos(\theta)}{k^4 + k^2 \tau} \sin(\alpha) \quad \text{parallel swimming.} \quad (\text{A11})$$

A similar symmetry argument, as given in Appendix A.1, shows which terms will survive the integration of (3.10). The same argument extends to cross-terms between the force and mass dipoles.

A.3. Active velocity dominated regime

Here, we present figures for the case where the active velocity dominates significantly over the singularity contributions, specifically, $|V_{act}| \gg (|D|/\eta h_0^2)$. We set

$$\frac{D}{\eta a^2} = 35|V_{act}|, \quad \frac{h_0}{a} = 50 \quad \text{and} \quad Q = 1. \quad (\text{A12})$$

The results are shown in figures 11 and 12. Notice that the velocity correction along z is not much different than what is presented in § 3.3. The magnitude of the correction is smaller as expected since the particle is essentially further away from the wall. However, along x , there are more pronounced differences compared with § 3.3. Specifically, for small incident angles, the particle's movement is enhanced in the positive x direction.

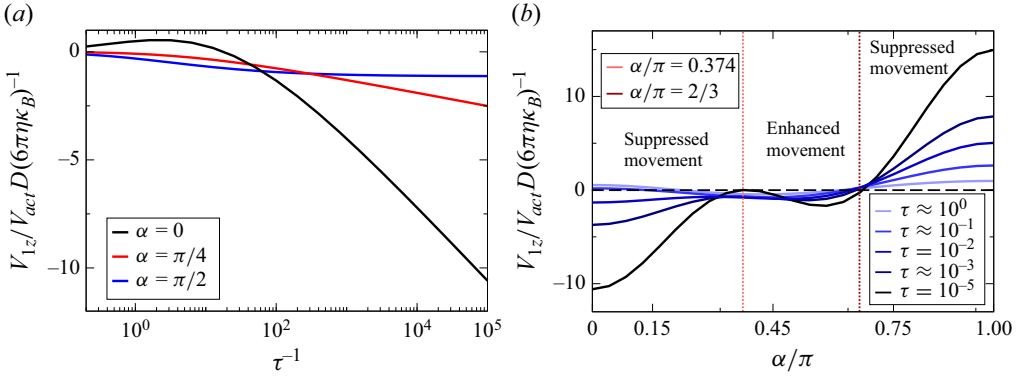


Figure 11. (a) Rescaled induced velocity along z of a self-propelled particle with force and mass dipole combination ($Q = 1$) as a function of dimensionless tension τ . Blue line is swimming parallel to the membrane, black line is perpendicular to membrane and red is swimming in $\alpha = \pi/4$. (b) Rescaled induced velocity along z of a force and mass dipole combination ($Q = 1$) as a function of orientation angle α .

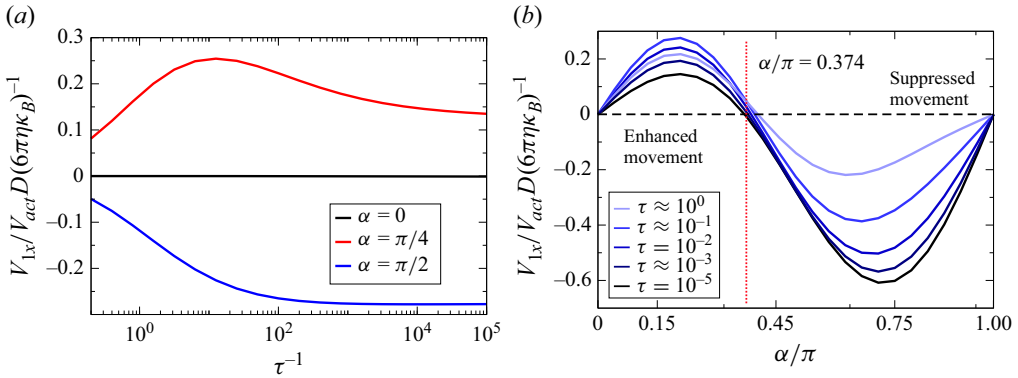


Figure 12. (a) Rescaled induced velocity along x of a self-propelled particle with force and mass dipole combination ($Q = 1$) as a function of dimensionless tension τ . Blue line is swimming parallel to the membrane, black line is perpendicular to membrane and red is swimming in $\alpha = \pi/4$. (b) Rescaled induced velocity along x of a force and mass dipole combination ($Q = 1$) as a function of orientation angle α .

A.4. Dominant force dipole ($Q \rightarrow 0$)

We now explore the different limits of the dipole ratio Q . First, consider the limit $Q \rightarrow 0$, where only the stresslet remains.

Correction to the normal velocity. The velocity correction along z as a function of dimensionless tension τ is shown in figure 13(a). For swimming with parallel, perpendicular and $\alpha = \pi/4$ orientations, the velocity scales as $\sim \log(\tau^{-1})$, while for the off-diagonal terms, the velocity correction is even smaller (see table 2). The dependence on α can be understood qualitatively using similar arguments as before. A stresslet is repelled from a rigid wall for small angles and is attracted to it for large angles. The cross-over between these regimes is given by setting $Q = 0$ in (3.15) and found to be $\alpha_{cross} = 0.3\pi \approx 0.95$ (dotted vertical line in figure 13b). For $\alpha < \alpha_{cross}$, the repulsion is suppressed since the membrane deforms away from the particle, while for $\alpha > \alpha_{cross}$, the attraction is enhanced since the membrane is pulled towards the particle. From symmetry, the dynamics along z is identical for $\alpha \in (\pi/2, \pi]$ as for $\alpha \in [0, \pi/2]$.

Direction	Singularity	Symmetry under $\phi \rightarrow \phi + \pi$	Correction direction and scaling
z	Parallel force dipole	+	$V_{1,z} \sim \frac{D^2}{\kappa_B \eta h^2} (0.15 \log(h\sqrt{T/\kappa_B}) + 0.04)$
	Perpendicular force dipole	+	$V_{1,z} \sim \frac{D^2}{\kappa_B \eta h^2} (0.59 \log(h\sqrt{T/\kappa_B}) + 0.19)$
	Off-diagonal terms	−	$V_{1,z} \sim \text{slower than } \frac{D^2}{\kappa_B \eta h^2} \log(h\sqrt{T/\kappa_B})$
	Force at $\alpha = \pi/4$	−	$V_{1,z} \sim \frac{D^2}{\kappa_B \eta h^2} (0.04 \log(h\sqrt{T/\kappa_B}) - 0.03)$
	Parallel mass dipole	−	$V_{1,z} \sim \text{slower than } \frac{q^2}{\kappa_B \eta h^3} \log(h\sqrt{T/\kappa_B})$
	Perpendicular mass dipole	+	$V_{1,z} \sim \frac{q^2}{\kappa_B \eta h^4} (0.79 \log(h\sqrt{T/\kappa_B}) + 0.25)$
	Mass dipole at $\alpha = \pi/4$	−	$V_{1,z} \sim \frac{q^2}{\kappa_B \eta h^4} (0.4 \log(h\sqrt{T/\kappa_B}) + 0.11)$
	Parallel force-mass dipoles	−	$V_{1,z} \sim \frac{D^2}{\kappa_B \eta h^2} (0.15 \log(h\sqrt{T/\kappa_B}) + 0.008)$
	Perpendicular force-mass dipoles	+	$V_{1,z} \sim \frac{D^2}{\kappa_B \eta h^2} (2.84 \log(h\sqrt{T/\kappa_B}) + 0.91)$
	Force-mass dipoles at $\alpha = \pi/4$	−	$V_{1,z} \sim \frac{D^2}{\kappa_B \eta h^2} (0.7 \log(h\sqrt{T/\kappa_B}) + 0.1)$
	Parallel self-propulsion	+	$V_{1,z} \sim \text{slower than } \frac{V_{act} D}{\kappa_B} (\log(h\sqrt{T/\kappa_B}))$
	Perpendicular self-propulsion	+	$V_{1,z} \sim \frac{V_{act} D}{\kappa_B} (4.05 \log(h\sqrt{T/\kappa_B}) + 6.86)$
	Self-propulsion at $\alpha = \pi/4$	−	$V_{1,z} \sim \frac{V_{act} D}{\kappa_B} (0.81 \log(h\sqrt{T/\kappa_B}) + 0.61)$

Table 2. Asymptotic results for velocity correction along z of different singularities.

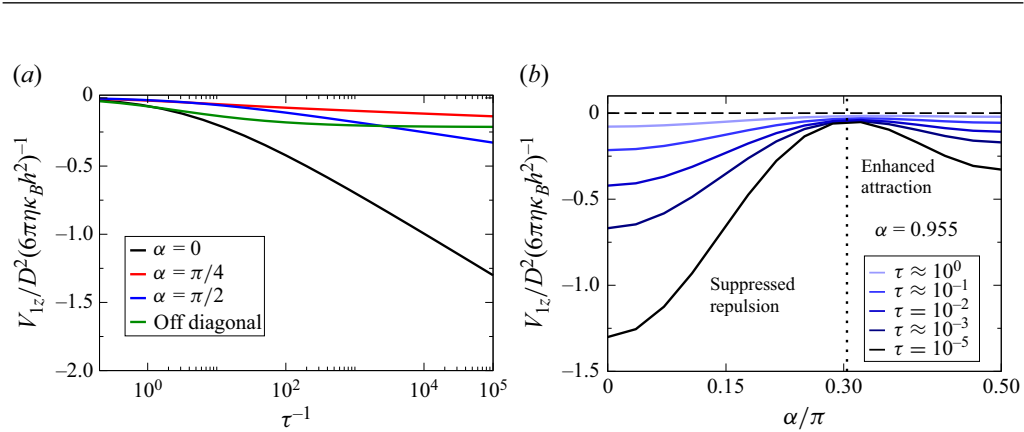


Figure 13. (a) Rescaled induced velocity along z of a stresslet ($Q = 0$) as a function of dimensionless tension τ . Blue line is swimming parallel to the membrane, black line is perpendicular to membrane, green line is off-diagonal terms only and red is swimming in $\alpha = \pi/4$. (b) Rescaled induced velocity along z of a stresslet as a function of orientation angle α .

Correction to the tangential velocity. Figure 14(a) shows the velocity correction along x of the different components of a stresslet as a function of the dimensionless tension τ . Notice that due to the symmetry of the problem, for each component separately, the velocity correction is zero, while the correction at $\alpha = \pi/4$ scales as $\sim \log(\tau^{-1})/h^2$. Figure 14(b) shows that for $\alpha \in (0, \alpha_{cross})$, the deformation suppresses motion in the

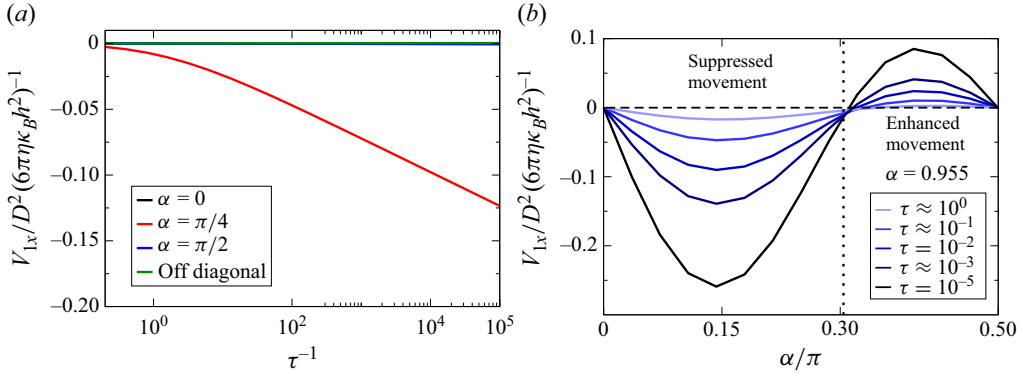


Figure 14. (a) Rescaled induced velocity along x of a stresslet ($Q = 0$) as a function of dimensionless tension τ . Blue line is swimming parallel to the membrane, black line is perpendicular, green line is off-diagonal terms only and red is swimming at $\alpha = \pi/4$. (b) Rescaled induced velocity along x of a stresslet as a function of orientation angle α .

positive x direction, while for $\alpha \in (\alpha_{cross}, \pi/2)$, the deformation enhances the motion. Lastly, we note that from a symmetry argument for $\alpha \in (\pi/2, \pi]$, we have that $V_{1,x}(\alpha) = -V_{1,x}(\pi - \alpha)$. Since in that range of α , the velocity V_0 is along negative x , the dynamics changes sign.

A.5. Dominant mass dipole ($Q \rightarrow \infty$)

We consider now the limit $Q \rightarrow \infty$, where only the mass dipole remains. Since now $D = 0$, a new velocity scale for the problem is chosen, specifically, $V_P = q(\eta h_0^3)^{-1}$ leading to $\Lambda = q(h_0 \kappa_B)^{-1}$. Therefore, the correction velocity due to deformation now scales as $V_1 \sim (q^2/\eta \kappa_B h^4)$. In this case, the cross-over angle according to (3.15) is $\alpha_{cross} = \pi/2$.

Correction to the perpendicular velocity. The results of the velocity correction along z as a function of dimensionless tension τ are shown in figure 15(a), where $V_1 \sim \log(\tau^{-1})/h^4$ or slower. Notice that the correction due to the parallel term is not identically zero but is much smaller than the correction due to the perpendicular component. The correction along z as a function of α is presented in figure 15(b). From (3.4), we see that the particle moves away from the membrane for $0 < \alpha < \pi/2$. Deformation suppresses this repulsion.

Correction to the parallel velocity. The results of the correction along x are presented in figures 16(a) and 16(b); see tables 2 and 3 for more details. For $0 < \alpha < \pi$, the movement of the mass dipole near a flat wall is along the positive x direction. Deformation suppresses this movement for $0 < \alpha < \pi/2$ and enhances it for $\pi/2 < \alpha < \pi$. Once more, this is consistent with (3.15), which predicts $\alpha_{cross} = \pi/2$.

A.6. Movement of a particle near a rigid flat wall

Here, we elaborate on the discussion around (3.4) about $V_{act} = 0$. The particle can either be attracted to the wall or repelled from it depending on the incident angle α . Specifically, we can set the velocity along z to be 0,

$$\left(\frac{3}{64} [2 \cos^2(\alpha) - \sin^2(\alpha)] + Q \frac{\cos(\alpha)}{8} \right) = 0, \quad (\text{A13})$$

to find where there is a transition from attraction to repulsion. Solving the above equation with $Q = 1$ gives $\alpha = 0.4\pi$. For $\alpha < 0.4\pi$, the particle is repelled from the wall and for

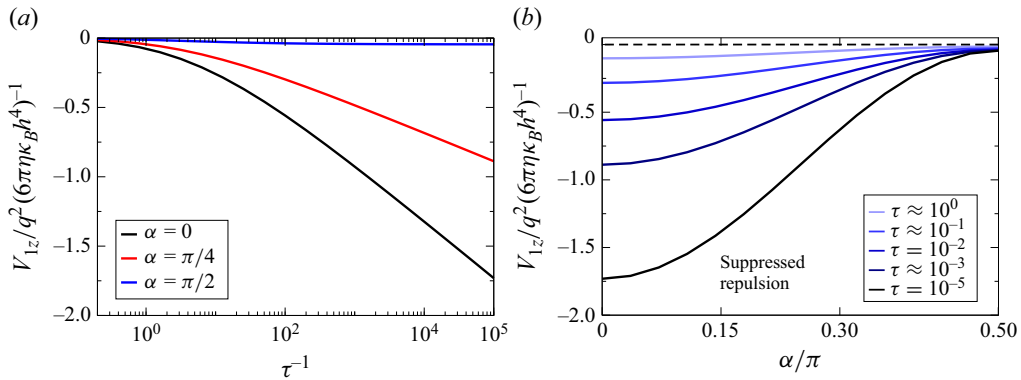


Figure 15. (a) Rescaled induced velocity along z of a mass dipole ($Q \rightarrow \infty$) as a function of dimensionless tension τ . Blue line is swimming parallel to the membrane, black line is perpendicular and red is swimming at $\alpha = \pi/4$. (b) Rescaled induced velocity along z of a mass dipole as a function of orientation angle α .

Direction	Singularity	Symmetry under $\phi \rightarrow \phi + \pi$	Correction direction and scaling
x	Parallel force dipole	+	$V_{1,x} = 0$
	Perpendicular force dipole	+	$V_{1,x} = 0$
	Off-diagonal terms	−	$V_{1,x} = 0$
	Force at $\alpha = \pi/4$	−	$V_{1,x} \sim \frac{D^2}{\kappa_B \eta h^2} (0.05 \log(h\sqrt{T/\kappa_B}) + 0.004)$
	Parallel mass dipole	−	$V_{1,x} = 0$
	Perpendicular mass dipole	+	$V_{1,x} = 0$
	Mass dipole at $\alpha = \pi/4$	−	$V_{1,x} \sim \frac{q^2}{\kappa_B \eta h^4} (0.1 \log(h\sqrt{T/\kappa_B}) + 0.23)$
	Parallel force-mass dipoles	−	$V_{1,x} \sim \frac{-D^2}{\kappa_B \eta h^2} (0.1 \log(h\sqrt{T/\kappa_B}) - 0.05)$
	Perpendicular force-mass dipoles	+	$V_{1,x} = 0$
	Force-mass dipoles at $\alpha = \pi/4$	−	$V_{1,x} \sim \frac{D^2}{\kappa_B \eta h^2} (0.33 \log(h\sqrt{T/\kappa_B}) + 0.49)$
	Parallel self-propulsion	+	$V_{1,x} \sim \text{slower than } \frac{V_{act} D}{\kappa_B} (\log(h\sqrt{T/\kappa_B}))$
	Perpendicular self-propulsion	+	$V_{1,x} = 0$
	Self-propulsion at $\alpha = \pi/4$	−	$V_{1,x} \sim \frac{V_{act} D}{\kappa_B} (0.16 \log(h\sqrt{T/\kappa_B}) + 0.28)$

Table 3. Asymptotic results for velocity correction along x of different singularities.

$\alpha > 0.4\pi$, it is attracted to it. Similarly, there is no motion along the wall (x direction), when

$$\left(\frac{3 \cos(\alpha) \sin(\alpha)}{32} + Q \frac{\sin(\alpha)}{32} \right) = 0. \quad (\text{A14})$$

The solution is now $\alpha = 0.61\pi$ for $Q = 1$: for smaller (larger) incident angles, the particle will move along $+x$ ($-x$). The total velocity of the particle near a flat wall with $V_{act} = 0$ is depicted in figure 4.

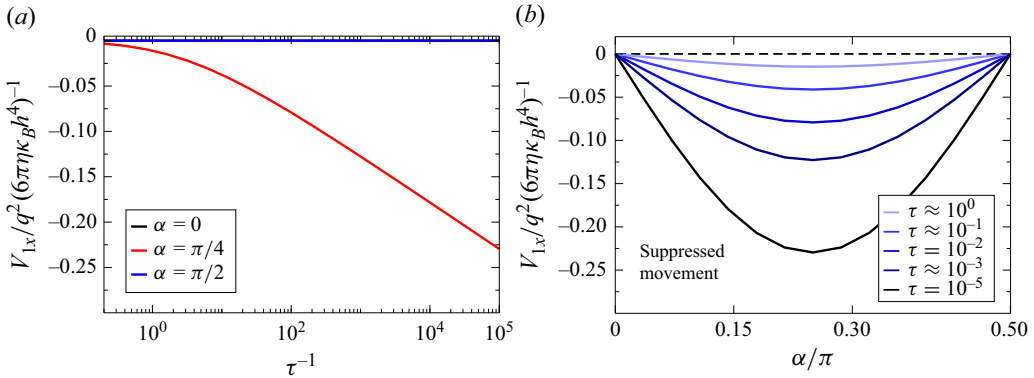


Figure 16. Rescaled induced velocity along x of a mass dipole ($Q \rightarrow \infty$) as a function of dimensionless tension τ . Blue line is swimming parallel to the membrane, black line is perpendicular to membrane and red is swimming in $\alpha = \pi/4$. (b) Rescaled induced velocity along x of a mass dipole as a function of orientation angle α .

REFERENCES

- ARUTKIN, M., LEDESMA-ALONSO, R., SALEZ, T. & RAPHAËL, É. 2017 Elastohydrodynamic wake and wave resistance. *J. Fluid Mech.* **829**, 538–550.
- BARBISH, J., TI, C., EKINCI, K. & PAUL, M.R. 2022 The dynamics of an externally driven nanoscale beam that is under high tension and immersed in a viscous fluid. *J. Appl. Phys.* **132** (3), 034501.
- BERKE, A.P., TURNER, L., BERG, H.C. & LAUGA, E. 2008 Hydrodynamic attraction of swimming microorganisms by surfaces. *Phys. Rev. Lett.* **101** (3), 038102.
- BLAKE, J.R. 1971 A note on the image system for a stokeslet in a no-slip boundary. *Math. Proc. Camb. Phil. Soc.* **70** (2), 303–310.
- BLAKE, J.R. & CHWANG, A.T. 1974 Fundamental singularities of viscous flow: part i: the image systems in the vicinity of a stationary no-slip boundary. *J. Engng Maths* **8** (1), 23–29.
- BUREAU, L., COUPIER, G. & SALEZ, T. 2023 Lift at low reynolds number. *Eur. Phys. J. E* **46** (11), 111.
- CHAKRABORTY, S., *et al.* 2020 How cholesterol stiffens unsaturated lipid membranes. *Proc. Natl Acad. Sci.* **117** (36), 21896–21905.
- DADDI-MOUSSA-IDER, A., GUCKENBERGER, A. & GEKLE, S. 2016 Long-lived anomalous thermal diffusion induced by elastic cell membranes on nearby particles. *Phys. Rev. E* **93** (1), 012612.
- DADDI-MOUSSA-IDER, A., LISICKI, M. & GEKLE, S. 2017 Mobility of an axisymmetric particle near an elastic interface. *J. Fluid Mech.* **811**, 210–233.
- DAVIES-STRICKLETON, H., DÉBARRE, D., EL AMRI, N., VERDIER, C., RICHTER, R.P. & BUREAU, L. 2018 Elastohydrodynamic lift at a soft wall. *Phys. Rev. Lett.* **120** (19), 198001.
- DIAS, M.A. & POWERS, T.R. 2013 Swimming near deformable membranes at low Reynolds number. *Phys. Fluids* **25** (10), 101901.
- DOMINO, L., FERMIGIER, M., FORT, E. & EDDI, A. 2018 Dispersion-free control of hydroelastic waves down to sub-wavelength scale. *Europhys. Lett.* **121** (1), 14001.
- DOWSON, D. & JIN, Z.-M. 1986 Micro-elastohydrodynamic lubrication of synovial joints. *Engng Med.* **15** (2), 63–65.
- DRESCHER, K., DUNKEL, J., CISNEROS, L.H., GANGULY, S. & GOLDSTEIN, R.E. 2011 Fluid dynamics and noise in bacterial cell–cell and cell–surface scattering. *Proc. Natl Acad. Sci.* **108** (27), 10940–10945.
- DREYFUS, R., BAUDRY, J., ROPER, M.L., FERMIGIER, M., STONE, H.A. & BIBETTE, J. 2005 Microscopic artificial swimmers. *Nature* **437** (7060), 862–865.
- DZWINEL, W., BORYCZKO, K. & YUEN, D.A. 2003 A discrete-particle model of blood dynamics in capillary vessels. *J. Colloid Interface Sci.* **258** (1), 163–173.
- ELFRING, G.J. & LAUGA, E. 2014 Theory of locomotion through complex fluids. In *Complex Fluids in Biological Systems: Experiment, Theory, and Computation*, pp. 283–317. Springer.
- FARES, N., LAVAUD, M., ZHANG, Z., JHA, A., AMAROUCHENE, Y. & SALEZ, T. 2024 Observation of Brownian elastohydrodynamic forces acting on confined soft colloids. *Proc. Natl Acad. Sci.* **121** (42), e2411956121.

- FEDOSOV, D.A., FORNLEITNER, J. & GOMPPER, G. 2012 Margination of white blood cells in microcapillary flow. *Phys. Rev. Lett.* **108** (2), 028104.
- FREUND, J.B. 2014 Numerical simulation of flowing blood cells. *Annu. Rev. Fluid Mech.* **46** (1), 67–95.
- FRYMIER, P.D., FORD, R.M., BERG, H.C. & CUMMINGS, P.T. 1995 Three-dimensional tracking of motile bacteria near a solid planar surface. *Proc. Natl Acad. Sci.* **92** (13), 6195–6199.
- GARAI, S., MAKANGA, U., VARMA, A. & KURZTHALER, C. 2025 Hydroelastic scattering and trapping of microswimmers. *Phys. Rev. Res.* **7** (4), L042005.
- GIMBUTAS, Z., GREENGARD, L. & VEERAPANENI, S. 2015 Simple and efficient representations for the fundamental solutions of Stokes flow in a half-space. *J. Fluid Mech.* **776**, R1.
- GREWE, J. & SCHWARZ, U.S. 2020 Mechanosensitive self-assembly of myosin II minifilaments. *Phys. Rev. E* **101** (2), 022402.
- GUCKENBERGER, A., KIHM, A., JOHN, T., WAGNER, C. & GEKLE, S. 2018 Numerical–experimental observation of shape bistability of red blood cells flowing in a microchannel. *Soft Matter* **14** (11), 2032–2043.
- HELFRICH, W. 1973 Elastic properties of lipid bilayers: theory and possible experiments. *Zeitschrift für Naturforschung c* **28** (11–12), 693–703.
- JHA, A., AMAROUCHENE, Y. & SALEZ, T. 2025 *Taylor’s Swimming Sheet Near a Soft Boundary*. *Soft Matter*.
JIN, Z. & DOWSON, D. 2005 Elastohydrodynamic lubrication in biological systems. *Proc. Inst. Mech. Eng., Part J: J. Engng Tribol.* **219** (5), 367–380.
- KARGAR-ESTAHBANATI, A. & RALLABANDI, B. 2021 Lift forces on three-dimensional elastic and viscoelastic lubricated contacts. *Phys. Rev. Fluids* **6** (3), 034003.
- KIM, S. & KARRILA, S.J. 2013 *Microhydrodynamics: Principles and Selected Applications*. Butterworth-Heinemann.
- KURZTHALER, C. & STONE, H.A. 2023 Hydrodynamics of cell swimming. In *Out-of-equilibrium Soft Matter* (ed. C. Kurzthaler, L. Gentile & H.A. Stone), chap. 2, pp. 32–87. The Royal Society of Chemistry.
- LAMPINEN, M.J. & NOPONEN, T. 2005 Electric dipole theory and thermodynamics of actomyosin molecular motor in muscle contraction. *J. Theor. Biol.* **236** (4), 397–421.
- LAUGA, E. 2020 *The Fluid Dynamics of Cell Motility*. Cambridge Texts in Applied Mathematics, vol. 62. Cambridge University Press.
- LAUGA, E., DI LUZIO, W.R., WHITESIDES, G.M. & STONE, H.A. 2006 Swimming in circles: motion of bacteria near solid boundaries. *Biophys. J.* **90** (2), 400–412.
- LEAL, L.G. 2007 *Advanced Transport Phenomena: Fluid Mechanics and Convective Transport Processes*. Cambridge University Press.
- LEDESMA-ALONSO, R., BENZAQUEN, M., SALEZ, T. & RAPHAËL, E. 2016 Wake and wave resistance on viscous thin films. *J. Fluid Mech.* **792**, 829–849.
- LEE, S., BUSH, J.W., HOSOI, A. & LAUGA, E. 2008 Crawling beneath the free surface: water snail locomotion. *Phys. Fluids* **20** (8), 082106.
- LORENTZ, H. 1896 Ein allgemeiner satz, die bewegung einer reibenden flüssigkeit betreffend, nebst einigen anwendungen desselben (a general theorem concerning the motion of a viscous fluid and a few consequences derived from it). *Versl. Kon. Akad. Wetensch* **5**, 168–174.
- LUSHI, E., KANTSLE, V. & GOLDSTEIN, R.E. 2017 Scattering of biflagellate microswimmers from surfaces. *Phys. Rev. E* **96** (2), 023102.
- MARCHETTI, M.C., JOANNY, J.-F., RAMASWAMY, S., LIVERPOOL, T.B., PROST, J., RAO, M. & SIMHA, R.A. 2013 Hydrodynamics of soft active matter. *Rev. Mod. Phys.* **85** (3), 1143–1189.
- MCWHIRTER, J.L., NOGUCHI, H. & GOMPPER, G. 2009 Flow-induced clustering and alignment of vesicles and red blood cells in microcapillaries. *Proc. Natl Acad. Sci.* **106** (15), 6039–6043.
- MIKHAILOV, A.S. & KAPRAL, R. 2015 Hydrodynamic collective effects of active protein machines in solution and lipid bilayers. *Proc. Natl Acad. Sci.* **112** (28), E3639–E3644.
- MOLAEI, M., BARRY, M., STOCKER, R. & SHENG, J. 2014 Failed escape: solid surfaces prevent tumbling of *escherichia coli*. *Phys. Rev. Lett.* **113** (6), 068103.
- MONTECUCCO, C. & RAPPUOLI, R. 2001 Living dangerously: how *helicobacter pylori* survives in the human stomach. *Nat. Rev. Mol. Cell Bio.* **2** (6), 457–466.
- MORIARTY, T.J., NORMAN, M.U., COLARUSSO, P., BANKHEAD, T., KUBES, P. & CHACONAS, G. 2008 Real-time high resolution 3d imaging of the lyme disease spirochete adhering to and escaping from the vasculature of a living host. *Plos Pathog.* **4** (6), e1000090.
- NAMBIAR, S. & WETTLAUER, J.S. 2022 Hydrodynamics of slender swimmers near deformable interfaces. *Phys. Rev. Fluids* **7** (5), 054001.
- NASOURI, B. & ELFRING, G.J. 2016 Hydrodynamic interactions of cilia on a spherical body. *Phys. Rev. E* **93** (3), 033111.

- OMORI, T., ISHIKAWA, T., BARTHÈS-BIESEL, D., SALSAC, A.-V., IMAI, Y. & YAMAGUCHI, T. 2012 Tension of red blood cell membrane in simple shear flow. *Phys. Rev. E—Stat., Nonlinear, Soft Matter Phys.* **86** (5), 056321.
- POZRIKIDIS, C. 2005 Axisymmetric motion of a file of red blood cells through capillaries. *Phys. Fluids* **17** (3), 031503.
- RALLABANDI, B. 2024 Fluid-elastic interactions near contact at low reynolds number. *Annu. Rev. Fluid Mech.* **56** (1), 491–519.
- RALLABANDI, B., OPPENHEIMER, N., BEN ZION, M.Y. & STONE, H.A. 2018 Membrane-induced hydroelastic migration of a particle surfing its own wave. *Nat. Phys.* **14** (12), 1211–1215.
- SAINTYVES, B., JULES, T., SALEZ, T. & MAHADEVAN, L. 2016 Self-sustained lift and low friction via soft lubrication. *Proc. Natl Acad. Sci.* **113** (21), 5847–5849.
- SECOMB, T.W. 2017 Blood flow in the microcirculation. *Annu. Rev. Fluid Mech.* **49** (1), 443–461.
- SECOMB, T.W., SKALAK, R., ÖZKAYA, N. & GROSS, J. 1986 Flow of axisymmetric red blood cells in narrow capillaries. *J. Fluid Mech.* **163**, 405–423.
- SEKIMOTO, K. & LEIBLER, L. 1993 A mechanism for shear thickening of polymer-bearing surfaces: elastohydrodynamic coupling. *Europhys. Lett.* **23** (2), 113.
- SKOTHEIM, J. & MAHADEVAN, L. 2004 Soft lubrication. *Phys. Rev. Lett.* **92** (24), 245509.
- SKOTHEIM, J. & MAHADEVAN, L. 2005 Soft lubrication: the elastohydrodynamics of nonconforming and conforming contacts. *Phys. Fluids* **17** (9), 092101.
- STONE, H.A. & DUPRAT, C. 2015 Low-reynolds-number flows. In *Fluid–Structure Interactions in Low-Reynolds-Number Flows*. The Royal Society of Chemistry.
- TANG, S., DAVOUDI, Z., WANG, G., XU, Z., REHMAN, T., PROMINSKI, A., TIAN, B., BRATLIE, K.M., PENG, H. & WANG, Q. 2021 Soft materials as biological and artificial membranes. *Chem. Soc. Rev.* **50** (22), 12679–12701.
- TROUILLOUD, R., YU, T.S., HOSOI, A. & LAUGA, E. 2008 Soft swimming: exploiting deformable interfaces for low reynolds number locomotion. *Phys. Rev. Lett.* **101** (4), 048102.
- WALKER, P., DOWSON, D., LONGFIELD, M. & WRIGHT, V. 1968 Boosted lubrication” in synovial joints by fluid entrapment and enrichment. *Ann. Rheum. Dis.* **27** (6), 512.
- WANG, Y., DHONG, C. & FRECHETTE, J. 2015 Out-of-contact elastohydrodynamic deformation due to lubrication forces. *Phys. Rev. Lett.* **115** (24), 248302.
- WITTEN, T.A. & DIAMANT, H. 2020 A review of shaped colloidal particles in fluids: anisotropy and chirality. *Rep. Prog. Phys.* **83** (11), 116601.
- ZHANG, Z., BERTIN, V., ARSHAD, M., RAPHAËL, E., SALEZ, T. & MAALI, A. 2020 Direct measurement of the elastohydrodynamic lift force at the nanoscale. *Phys. Rev. Lett.* **124** (5), 054502.